International Journal of Infrared and Millimeter Waves, Vol. 27, No. 4, April 2006 (© 2006)
DOI: 10.1007/s10762-006-9106-7

TERAHERTZ QUALITY CONTROL OF POLYMERIC PRODUCTS

Frank Rutz and Martin Koch

Institut für Hochfrequenztechnik
Technical University of Braunschweig
38106 Braunschweig, Germany

Shilpa Khare and Martin Moneke

German Institute for Polymers (DKI)
64289 Darmstadt, Germany

Heike Richter and Uwe Ewert

Federal Institute for Materials Research and Testing (BAM)
12200 Berlin, Germany

Abstract

We report on experiments that evaluate the potential of terahertz (THz) time-domain spectroscopy (TDS) for quality control of polymeric compounds. We investigate specimens out of a polyethylene compound with silver-coated titanium dioxide nanospheres and a glass-fiber reinforced epoxy composite. We further examine an industrial polymer product produced by injection molding. Our data demonstrates that THz imaging is a powerful tool for contactless quality control in the polymer industry.

Keywords: Terahertz (THz), time-domain spectroscopy (TDS), polymers, quality control

I Introduction

Most polymers are largely transparent for terahertz (THz) waves. This can be used by the polymer industry for an inline quality control of polymeric products in two ways. Firstly, the polymer parts produced by injection moulding can be inspected so as to find out whether their dimensions are within the fabrication tolerances. Mostly, a hundred percent inspection is desired but often difficult to implement with existing methods. Secondly, polymeric compounding processes can be monitored. During this process organic or inorganic fillers or additives are mixed with a polymer to modify its physical properties according to the customer's demands. To achieve the desired properties with a minimum amount of additives and fillers an optimum dispersion is required.

In this paper we demonstrate that THz imaging [1-6] using THz pulses can be used to determine the degree of dispersion, to visualize inhomogeneities in fiber-reinforced plastics and to measure the dimensions of injection moulding parts.

II Experimental Setup

For our experiments we use a standard THz time-domain transmission spectrometer (Fig. 1). Ultra-short current pulses are generated by femtosecond laser pulses in photoconductive antennas. The emitter antenna consists of a coplanar stripline on a GaAs substrate. An applied bias voltage of 40 V causes an acceleration of the free carriers generated by the incident laser pulses. These current pulses act as a source for broadband THz pulses. Four off-axis parabolic mirrors guide the THz wave which is detected by another coplanar stripline on a silicon-on-sapphire substrate, that also includes a small dipole structure. This time, the generated free carriers are accelerated by the electric field of the incoming THz wave. The resulting photocurrent is measured with a lock-in amplifier. By delaying the laser pulses of the emitter and detector arm with respect to each other, the THz waveform can be sampled (see [1-3] for details).

The sample under investigation is placed in an intermediate focus between the emitter and detector antenna. In order to obtain the absorption spectrum of the sample, the frequency content of the transmitted THz pulse is compared to a reference spectrum. For imaging measurements, the sample is scanned in the x and y directions perpendicular to the THz beam through the intermediate focus [1-3].

For every position a waveform is sampled and analyzed. For example one can analyze the amplitude of the THz pulse or its temporal position [7]. Often the waveform is Fourier transformed and the transmitted intensity in a frequency interval to be chosen is determined. In any case, the result of this analysis is condensed into one value which represents the pixel of an image. Depending on the method of analysis, the THz image contains different information.

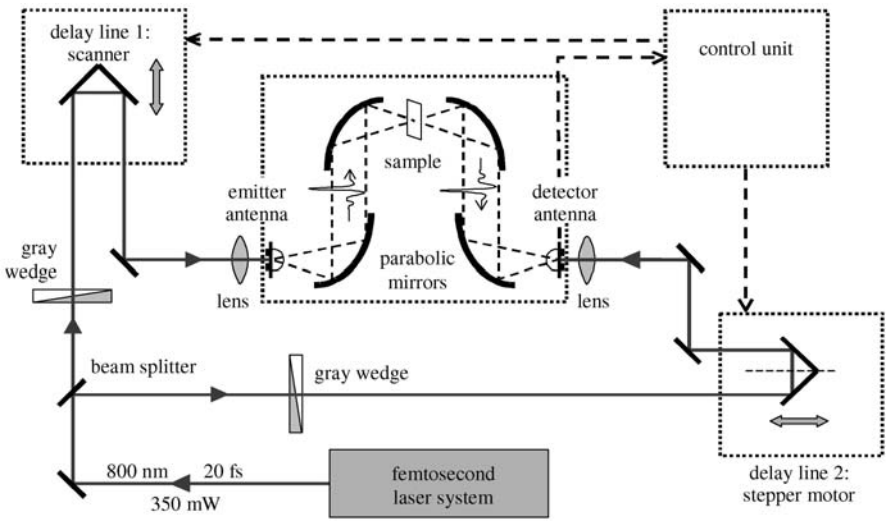

Fig.1: Experimental setup for terahertz time-domain spectroscopy.

III Samples

To illustrate the potential of THz imaging for the quality control of polymeric products we investigate three samples.

The first sample is a low-density polyethylene (LDPE) containing 5 wt% of Ag-TiO_2 nanofiller. This filler consists of TiO_2-nanospheres with a mean diameter of 270 nm. These spheres are themselves coated with silver nanoparticles which are even smaller (typical diameter of 10 - 20 nm) than the aforementioned nanospheres. The total Ag mass fraction is 0.05 wt%. Since Ag ions tend to diffuse from the nanoparticles through the polymeric matrix to the product surface, an antimicrobial effect occurs. This can be utilized for the development of self-disinfecting plastic products, e.g. door handles or food containers. However, a good dispersion of Ag-nanoparticles is required for the controlled release of silver ions from the polymer, which ensures a long term antimicrobial effect. Also, other material parameters like the mechanical stability can suffer from such functional additives, especially if the variation of the filler distribution exceeds a certain threshold. Hence, the proper dispersion of the filler in polymeric compounds is a critical measure in the quality control of the compounding process.

Secondly, we investigate tensile specimen of fiber reinforced plastics (FRP), in our particular case glass-fiber laminates (GFRP) made from an epoxy matrix with included woven glass-fiber fabrics of linen-style as a 0°/90°-laminate (sample A) and a +/–45°-laminate (sample B) in the virgin state. We also investigate a fractured specimen similar to sample B, which has already been tested in tensile loading (sample C). The matrix material epoxy is a resin, which in the cured state is a duroplastic polymer. The fiber reinforcement is stabilized in position by the matrix which gives a composite of a low weight as well as a high chemical stability. With unidirectional reinforcement, glass-fiber-composites can reach a tensile strength of about 700 to 1000 MPa. The direction of the fiber-reinforcement for the decisive component depends on its usage purpose. For instance, a +/–45°-laminate is utilized for parts which exhibit shearing strains. The main applications of GFRPs are not only in transportation systems like aircraft, railway and automotive, but also for wind-turbine-blades. For the quality control of FRP it is essential to gain insight into the inner structure of the laminate material, in particular to detect delaminating, micro cracking like matrix de-bonding and matrix cracking, as well as to determine the fibers orientation in the matrix material.

The third example is the cover of a car airbag. It illustrates the potential of THz imaging to determine the dimensions of injection moulding parts.

IV Results and Discussion

LDPE/Ag-TiO_2 compounds

Fig. 2 shows a photograph and a THz transmission image of the LDPE/Ag-TiO_2 sample obtained for the frequency range from 0.4 to 0.5 THz. The image shows regions of enhanced transmission of more than 25 %, mainly located in two horizontal bands at y = 5 mm and 9 mm. The photograph reveals a slight surface roughness in the scanned region indicated by the frame in Fig. 2a. However, a

manually made artificial dent does not occur in the THz image although it is much deeper than the little dents forming the natural surface roughness. Hence, we can conclude that the inhomogeneities observed in the THz image do not arise from refraction off the somewhat rough sample surface [8].

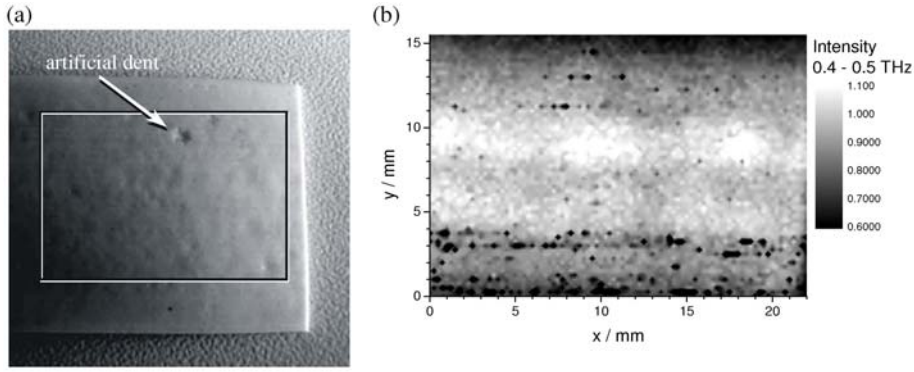

Fig.2: (a) Photograph and (b) THz image of the LDPE sample.

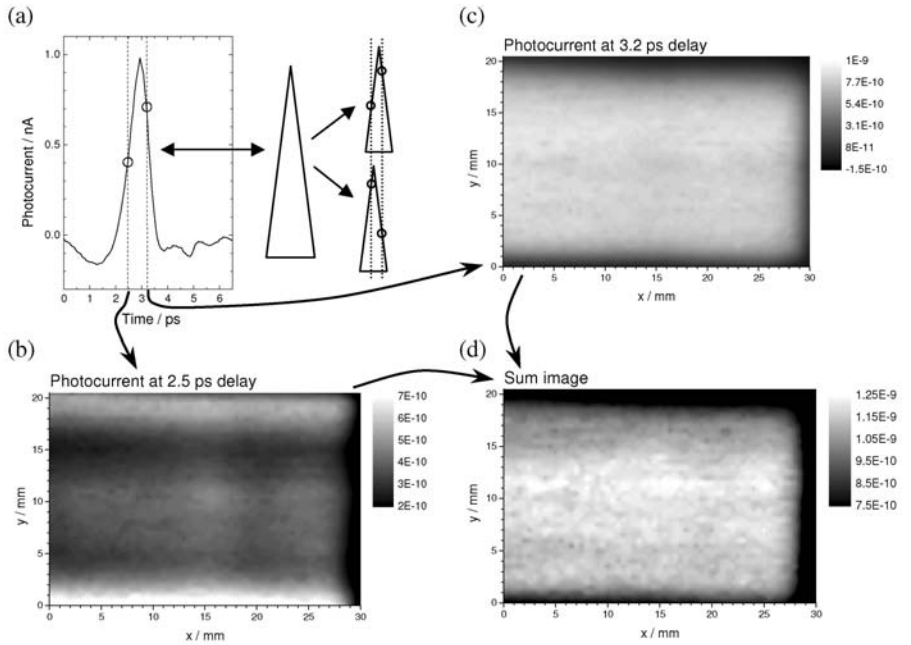

Fig.3: (a) THz waveform after propagation through the sample. The shape of the peak resembles that of a isosceles triangle. Images (b) and (c) are obtained from the photocurrent of the transmitted THz pulse at a fixed time delay. (d) Sum of the two images showing basically the same features as in the intensity image of Fig. 2 (b).

To verify that the structures in the THz image are not due to the change of the thickness, we followed a second imaging procedure. This time, we use a fixed time delay of the gating detector laser pulse and take a THz image by measuring the photocurrent. In Fig. 3 a THz waveform (a) is plotted. The delays at which two consecutive images of the sample are obtained are indicated by the two circles. The time delays are 2.5 and 3.2 ps for image (b) and (c), respectively. Since the measurements are performed in the flanks of the THz pulse, both absorption and a temporal shift of the pulse will alter the photocurrent. Assuming that the THz peak has roughly the shape of an isosceles triangle, the effect of a temporal pulse shift vanishes by adding up two images taken at the front and back flanks of the pulse. This works if the temporal shift is small in comparison to the pulse duration. Such a sum image is presented in Fig. 3 (d). The observed structures are basically identical to that in Fig. 2 (b). Hence, we can exclude thickness variations from being responsible for the observed features. We conclude that the variations in the sample transmission arise either from inhomogeneities in the absorption coefficient resulting from an inhomogeneous filler concentration or from locally varying scattering properties due to an inhomogeneous agglomeration of the nanoparticles.

It is known that nanoparticles tend to form agglomerates up to the scale of micrometers. This can be seen in Fig. 4 which shows two transmission electron microscopy (TEM) images of LDPE containing the nanofiller TiO_2. Each black spot corresponds to a TiO_2 sphere coated with silver. The images are taken at the German Institute for Polymers (DKI), where the problem of dispersion vs. agglomeration in polymeric nanocompounds is well known. Local variations in the size and distribution of such agglomeration centres would lead to inhomogeneities of the scattering strength.

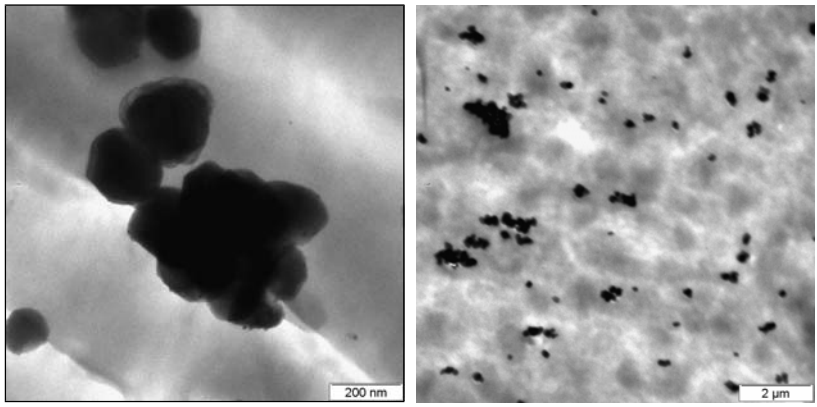

Fig.4: Transmission electron microscopy (TEM) images of a LDPE sample containing the nanofiller TiO_2.

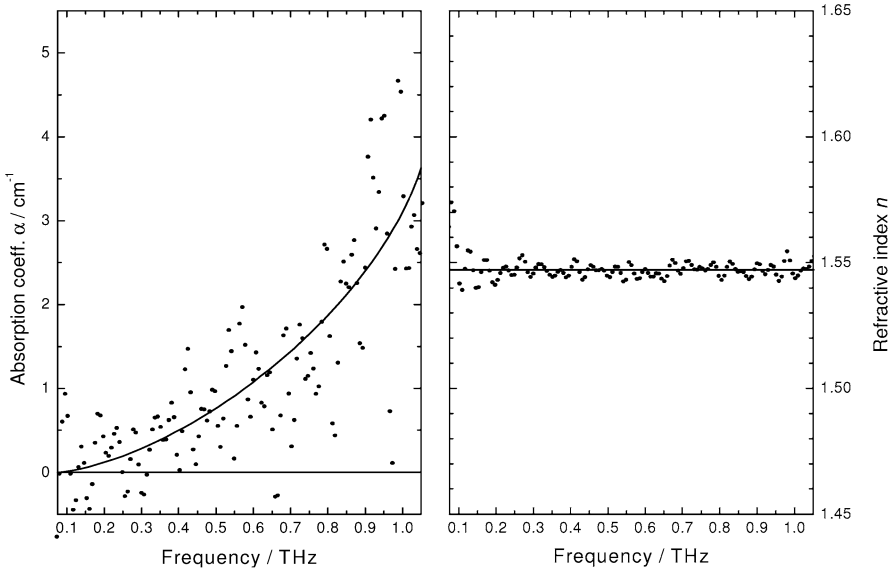

Fig.5: Absorption coefficient and refractive index of LDPE + 5 wt% Ag-TiO_2.

The corresponding absorption curves are not conclusive. Fig. 5 shows the absorption coefficient and refractive index of the sample. The small sample thickness of approximately $d = 1.35$ mm and the low filler concentration makes it difficult to obtain smooth curves since Fabry-Perot resonances and system noise affect the data processing significantly. Yet, it is obvious that the nanofiller causes a deviation from the values of pure LDPE of $\alpha < 1$ cm^{-1} and $n = 1.52$. Unfortunately, it is difficult to quantitatively separate the contribution to the absorption curve arising from pure absorption from that resulting from scattering effects. The shape of the absorption curve is typical for a sample where scattering losses dominate, but this argument is too weak to draw a definite conclusion. From Figs 2 (b) and 3 (d) we know that the "absorption strength" varies over the sample plane but it cannot be answered in this case if this arises from an inhomogeneous filler concentration or from an inhomogeneous agglomeration of the nanoparticles.

Nevertheless, our data clearly shows that inhomogeneities in polymeric compounds can be detected using THz imaging (see also [9]).

B Glass-fiber reinforced epoxy

In contrast to the polymer compound with nanofillers, glass-fiber reinforced polymers (GFRPs) might provide anisotropic THz properties due to alignment of the fibers. The samples consist of eight woven layers of linen-style fiber fabrics as schematically illustrated in Fig. 6. The single fibers have a diameter of 11 µm. They are bundled together to typically 2 mm wide bands which are woven to linen-style nettings.

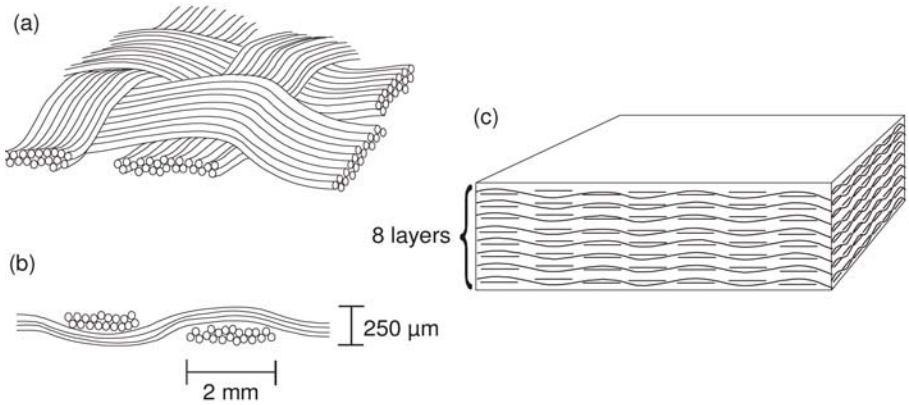

Fig.6: Schematic of the linen-style fiber network in steric view (a) and section (b). The 11 µm thick glass-fibers form flat bundles of 2 mm width that are woven to approximately 250 µm thick nettings. A stack of 8 fiber netting layers within a epoxy matrix results in a 2 mm thick tensile specimen.

The absorption coefficients and the refractive indices of the GFRP samples A, B, and C are plotted in Fig. 7. No significant difference in the absorption coefficients between the three samples are observed, although the linen-style fiber network differs from 0°/90° alignment (sample A) to +/– 45° (samples B and C). All absorption curves are rather smooth with the exception of experimental noise, a water line at 550 GHz and an absorption peak at 275 GHz which we attribute to interference arising from multiple reflections between the different layers of the fiber fabric.

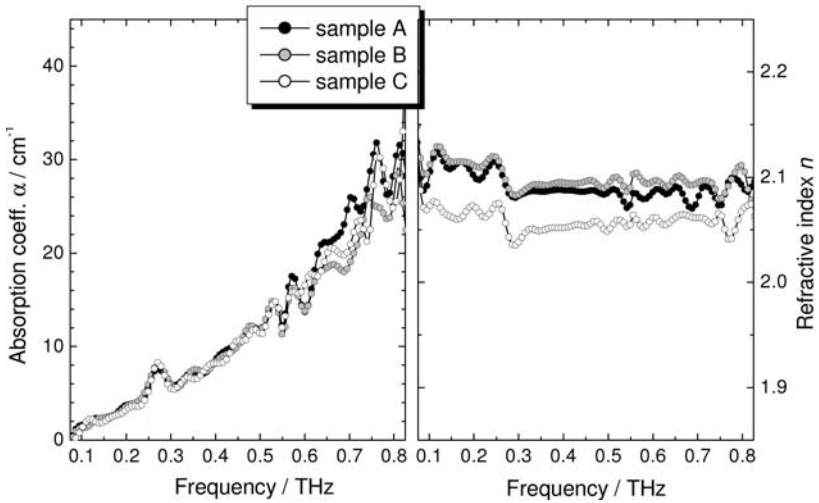

Fig.7: Refractive index and absorption coefficient of three similar glass-fiber reinforced epoxy specimen.

The refractive index for all samples is comparable. Yet, it is somewhat smaller for sample C which we find to be a bit thicker (2.06 mm) than the samples A and B (2.00 mm). We attribute this increase in thickness to little cracks induced by the tensile strength test. Hence, the sample contains tiny air cavities which lower the mean refractive index.

Fig. 8 shows a photograph of the sample together with two THz transmission images of sample C obtained for frequency ranges of 0.3 – 0.4 THz (b) and 0.5 – 0.75 THz (c). In the lower frequency window only cloudy structures are observed (Fig. 8 (b)). We attribute these structures to cracks resulting from the tensile strength test. The image obtained for higher frequencies additionally shows the structures of the fiber network. The shorter wavelength corresponding to the higher frequency can resolve the fine structure of the network.

This example shows that structures buried within a polymer can be visualized in a THz transmission image. Also mechanical damages are detected.

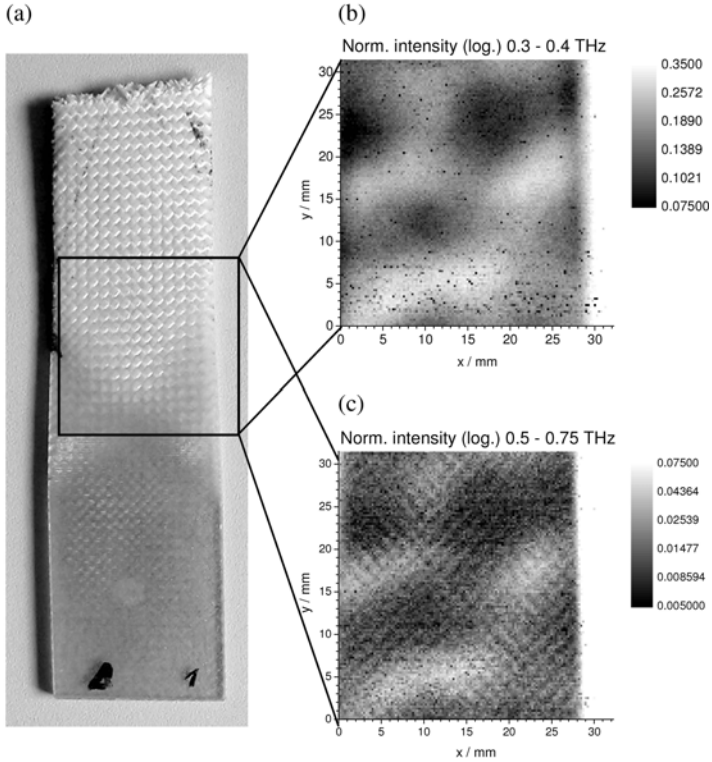

Fig.8: Photograph and THz transmission images of a glass-fiber reinforced epoxy specimen (sample C).

C Airbag cover

Figure 9 (a) shows an airbag lock. In the given photo one can discern the creases where the material is thinner. Along these creases the lock will break off and the airbag will spring out. Therefore the thickness of the material is a critical element. When the material is too weak, the passenger can accidentally damage the cover. If the material is too strong, the clamp will not dislodge and the cover may shoot out at full force and injure the occupant. Since the airbag with its cover is a part of the car's safety system the best possible compliance with the tolerance requirements for the groove depth is crucial. Hence, a non-destructive, non-contacting, but reliable test method for the material thickness is desired. The end-goal would be 100 % control, where each produced piece is inspected.

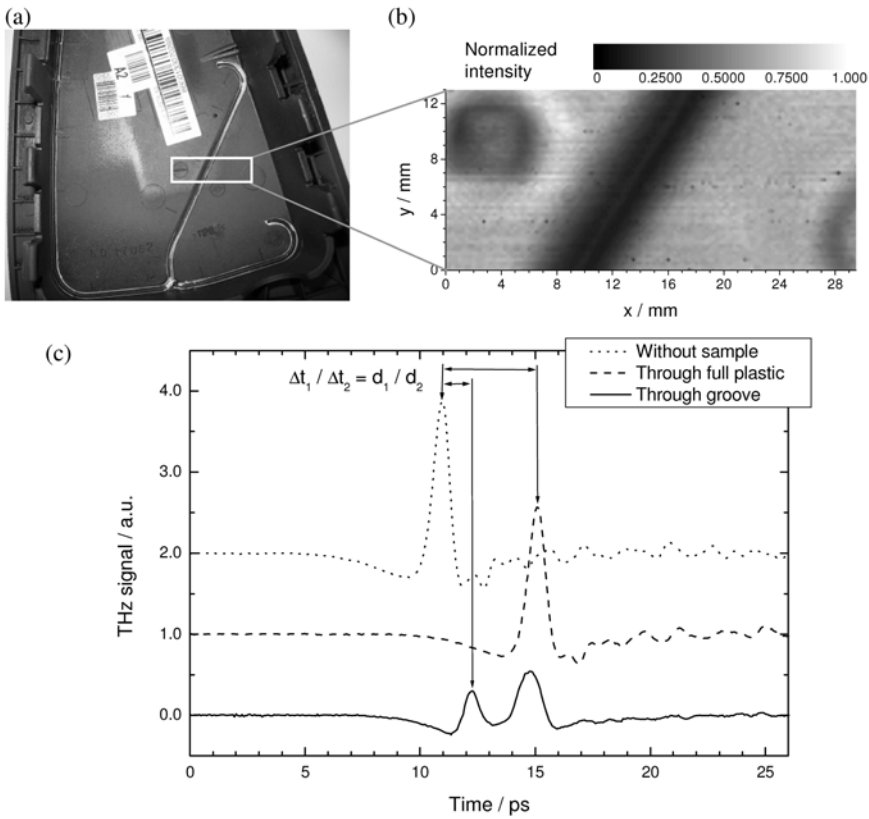

Fig.9: (a) Photograph of the back side of an airbag cover, (b) THz transmission image of a part of the cover, (c) selected THz waveforms, vertical offset for clarity.

In image 9 (b) creases can be observed. The material strength can be evaluated by using the peak position of the THz pulse. Fig. 9 (c) shows as a dotted line a THz-pulse travelling simply through the air. The dashed line shows the waveform when it travels through an area in the clamp in the vicinity of the creases. The solid line shows the curve that results when a pulse is propagated through a crease. This later curve has two signal peaks, the smaller of which being the most relevant. Through a comparison between this curve and the dotted curve the material strength can be precisely measured. This example shows how a THz system can be used to determine the strength of a certain material. THz imaging can also be used to measure the dimensions of injection moulding parts with more complicated geometries. In particular multi-layered structures with air layers in between can be measured, a task that is difficult for ultrasound [2].

Acknowledgment

We thank Dr. Trappe from the Federal Institute for Materials Research and Testing (BAM) in Berlin, Germany, for providing the fiber reinforced polymer samples.

References

[1] B.B. Hu, M.C. Nuss, "Imaging with terahertz waves", Opt. Lett. **20**, 1716-1718 (1995).

[2] S. Hunsche, D. M. Mittleman, M. Koch, M. C. Nuss, "New Dimensions in T-Ray Imaging", *IEICE Trans. Electron.* **E81-C**, 269 (1998).

[3] D.M. Mittleman, M. Gupta, R. Neelamani, R.G. Baraniuk, R.G. Rudd, M. Koch, "Recent Advances in Terahertz Imaging", Appl. Phys. B **68**, 1085-1094 (1999).

[4] K. Kawase, Y. Ogawa, Y. Watanabe, and H. Inoue, "Non-destructive terahertz imaging of illicit drugs using spectral fingerprints", Opt. Expr. **11**, 2549-2554 (2003).

[5] C. Zandonella, "T-ray specs", *Nature*, **424**, 721 (2003).

[6] D.M. Mittleman (ed.), "Sensing with Terahertz Radiation", Springer-Verlag, Heidelberg (2003).

[7] M. Herrmann, M. Tani, K. Sakai, "Display Modes in Time-Resolved Terahertz Imaging", Jpn. J. Appl. Phys. **39**, 6254-6258 (2002).

[8] F. Rutz, M. Koch, S. Khare, M. Moneke, "Quality control of polymeric compounds using terahertz imaging", Proc. SPIE Int. Soc. Opt. Eng., **5727**, 115 (2005).

[9] F. Rutz, M. Koch, K. Kretschmer and M. Bastian, "Terahertz imaging as a new tool to study dispersion in polymeric compounds", Proc. ANTEC2005 Soc. Plastics Eng., sec. T38, 3645 (2005).